Bioelectrochemistry 86 (2012) 46–53

Contents lists available at SciVerse ScienceDirect

Bioelectrochemistry

journal homepage: www.elsevier.com/locate/bioelechem

TiC nanoparticles-chitosan composite film for the direct electron transfer of myoglobin and its application in biosensing

Minzhi Wang, Qinglin Sheng, Dawei Zhang, Yaping He, Jianbin Zheng *

Institute of Analytical Science / Shaanxi Provincial Key Laboratory of Electroanalytical Chemistry, Northwest University, Xi'an, Shaanxi 710069, China

ARTICLE INFO

Article history:
Received 20 August 2011
Received in revised form 15 January 2012
Accepted 21 January 2012
Available online 1 February 2012

Keywords:
Myoglobin
TiC nanoparticles
Direct electrochemistry
Electrocatalysis
Biosensor

ABSTRACT

We report on the direct electrochemistry of myoglobin (Mb) immobilized on a composite matrix based on chitosan (CHIT) and titanium carbide nanoparticles (TiC NPs) underlying on glassy carbon electrode (GCE). The cyclic voltammetry and electrochemical impedance spectroscopy were used to characterize the modified electrode. In deaerated buffer solutions, the cyclic voltammetry of the composite films of Mb-TiC NPs-CHIT showed a pair of well-behaved redox peaks that are assigned to the redox reaction of Mb, confirming the effective immobilization of Mb on the composite film. The electron transfer rate constant was estimated to be 3.8 ($\pm$0.2)$\cdot s^{-1}$, suggested that the interaction between the protein and certain electrode surfaces may mimic some physiological situations and may elucidate the relationship between the protein structures and biological functions. The linear dynamic range for the detection of hydrogen peroxide was 0.5–50 μM with a correlation coefficient of 0.999 and the detection limit was estimated at about 0.2 μM (S/N = 3). The calculated apparent Michaelis–Menten constant was 0.07 ($\pm$0.01) mM, which suggested a high affinity of the redox protein–substrate. The immobilized Mb in the TiC NPs-CHIT composite film retained its bioactivity. Furthermore, the method presented here can be easily extended to immobilize and obtain the direct electrochemistry of other redox enzymes or proteins.

1. Introduction

In recent years, the direct electron transfer (DET) of biologically important proteins has become one of the hottest research areas due to its significance in both theoretical and practical application [1,2]. Bernhardt [3] et al. have studied the direct electrochemistry of non-heme diiron enzyme porcine purple acid phosphatase (uteroferrin, Uf) and was further used for calculation of acid dissociation constants for Uf and its phosphate and arsenate complexes to understand the role of these interesting metalloenzymes and their mechanism. Pulcu [4] et al. have been extensively investigated the direct electrochemistry of heme proteins and revealed that the source of the cooperativity of cytochrome c554 protein does not appear to be related to intermolecular interactions, but could be achieved by the relative kinetics of interfacial and intramolecular electron transfer events. Sadeghi [5] et al. described the first direct electrochemistry of human flavin-containing monooxygenase that catalyzes the oxygenation of a wide range of nitrogen- and sulfur-containing drugs to identify Benzydamine and Tamoxifen drugs. Periasamy [6] et al. have fabricated a sensitive glucose biosensor based on the direct electrochemistry of glucose oxidase at gelatin-multiwalled carbon nanotube modified electrode, which showed good anti-interference ability and was successfully applied for glucose detection in human serum samples. It can provide a good model not only for study of the important information about the dynamic characteristics in biological systems, but also for probing the biosensing properties of a combination of biological macromolecules and designing new kinds of label-free biosensors or biomedical devices [7–12].

Heme-based proteins such as hemoglobin (Hb), myoglobin (Mb), horseradish peroxidase (HRP), and cytochrome c (Cyt c) have been investigated. Among those proteins, Mb is generally used as a model for the direct electron transfer process between redox proteins and the modified electrode in the biological systems, due to the advantages of commercial availability, well-documented structure and excellent electrocatalytic abilities. However, the DET between the redox proteins and the bare solid electrode is usually slow because the electroactive centers of proteins are deeply buried in its structure and the proteins are easy to be irreversibly denatured [13–15]. To solve this problem, several valuable immobilization strategies such as adsorption [16], cross-linking [17], and layer-by-layer assembly [18] have been successfully used for the immobilization of proteins on electrode surfaces. Entrapment or encapsulation of proteins within a biocompatible material by using simple procedures, especially physical entrapment of biomolecules without the need of complicated covalently attachment, is certainly desirable. Among various biocompatible materials, chitosan (CHIT), a versatile biopolymer, has been widely used as an immobilization matrix for biosensors and biocatalysis [19,20]. The combination of nanomaterials and CHIT can

* Corresponding author. Tel.: +86 29 88302077; fax: +86 29 88303448.
E-mail address: zhengjb@nwu.edu.cn (J. Zheng).

1567-5394/$ – see front matter © 2012 Elsevier B.V. All rights reserved.
doi:10.1016/j.bioelechem.2012.01.009

create unique materials that have open up new opportunities for the study of DET of important redox proteins and the construction of biosensors [21,22].

Besides, the acceleration of electron transfer rate is another aspect to be considered. One of the most exciting recent developments is the application of nanomaterials because of their excellent conductivity, biocompatibility and optical-electronic properties [23–28]. Deng [24] et al. has reported the DET of Superoxide Dismutase based on ZnO nanodisks and its application in vivo detection of superoxide anion in bean sprout. Xiao [25] et al. has reported the fabrication of H_2O_2 biosensor by immobilizing HRP into a CeO_2 nanocubes modified electrode. Other nanomaterials, such as niobium pentoxide [26], tungsten oxide [27], mesoporous carbon [28] and lanthanum phosphate [29] have been used successfully for immobilization of enzymes and proteins. Those studies have showed that the new nanomaterials exhibit high biocompatibility, high adsorption ability and little harm to the biological activity of redox proteins. Transition metal carbides have attracted significant interest for a number of applications due to intrinsic material properties such as excellent thermal and chemical stability, corrosion resistance, and metal-like conductivity [30]. Being a representative example of these materials, titanium carbides (TiC) exhibit high electrical conductivity, low density, high surface area and catalytic activity [31–34], which has been considered as an electrode material for sensing of Pb^{2+} ion [35]. Recently, TiC was explored as a negative electrode for the electro-oxidation of borohydride/ ammonia borane in alkaline media for fuel cell [36]. Moreover, nanosized TiC shows greater advantages and novel characteristics than regular sized particles, such as the much larger specific surface area and high electron transfer rate. Liu [37] et al. have demonstrated that TiC can be served as a favorable ion-path for electrolyte penetration and allowing for fast ionic transport and good electronic conductivity, thus show an excellent capacitance retention at high discharge rates for pulse power applications. Brama [38] et al. have coated TiC on titanium substrates to evaluate the biological response both in vitro and in vivo. They found that the expression of genes central to osteoblast differentiation, such as alkaline phosphatase and osteocalcin, were up-regulated in all cell lines grown on TiC, whilst genes involved in modulation of osteoclastogenesis and osteoclast activity were unchanged. Similar to TiC, another metal carbide, tungsten carbide was found that can accelerate the electron transfer between conductive bacterial and the electrode, which was successfully used for a high-performance, noble-metal-free microbial fuel cell construction [39]. These properties may provide favorable conditions for enzyme or protein immobilization.

Previous studies have shown that the interaction between the protein and certain electrode surfaces may mimic some physiological situations and may elucidate the relationship between the protein structures and biological functions [40,41]. In this work, we describe the direct electrochemistry of Mb immobilized on TiC NPs-CHIT composite matrix. The electrochemical behaviors of the composite film are thoroughly investigated by cyclic voltammetry and electrochemical impedance spectroscopy. The resulting biosensor can catalyze the reduction of hydrogen peroxide (H_2O_2) and was used for sensitive determination of H_2O_2. Accordingly, the TiC NPs-CHIT composite matrix can be applied as a useful material for the design of enzymatic biosensors and bioelectronics based on bioelectrochemistry.

2. Experimental

2.1. Reagents

Bovine myoglobin (Mb, MW. 64500) was purchased from Sigma and used without further purification. TiC powders (>99% purity, 40 nm in diameter) were purchased from Kaier Company (China). H_2O_2 (30%, w/v) and potassium hexacyanoferrate were of analytical grades and used without further purification. CHIT (MW 1×10^6, >90% deacetylation) was purchased from Shanghai Xiangsheng Biotechnology Co., Ltd. (China). All solutions were prepared with ultrapure water (>18 MΩ·cm) obtained from a Millipore Milli-Q water purification system.

2.2. Apparatus

A Model CHI660D Electrochemistry Workstation (Chenhua Instruments in Shanghai, China) was employed for all the electrochemical techniques. A three-electrode system, where a standard saturated calomel electrode (SCE) served as reference electrode, a platinum wire electrode as the auxiliary electrode, and the prepared electrodes as the working electrode. All the electrochemical experiments were conducted at room temperature. For Fourier-transform infrared (FTIR) spectral studies, the Mb-TiC NPs film was prepared by dropping Mb-TiC NPs suspension onto ITO surface and dried at 4 °C in a refrigerator to make Mb-TiC NPs/ITO sample. The Mb-TiC NPs film was scraped carefully, and then the FTIR spectra of Mb and Mb-TiC NPs were recorded by using KBr pellets of the samples on a Nicolet 380 FTIR Spectrometer (Thermo electron corporation, USA). UV–vis spectra were recorded using a UV-2501PC spectrophotometer (Shimadzu, Japan). Indium tin oxide (ITO) substrates with sheet resistance ≤10 Ω/cm from CSG Holding Co., LTD., (Shenzhen, China) were used and cleaned by acetone in an ultrasonic bath for 10 min before use. The Mb and Mb-TiC NPs-CHIT suspension with concentration of 1 mg/mL, then 200 μL of this suspension was uniformly dropped onto ITO with 160 cm^2 areas and dried at room temperature to make Mb/ITO and Mb-TiC NPs-CHIT/ITO sample. With ITO as the reference, the UV–vis spectra of Mb and Mb-TiC NPs-CHIT were detected using UV–vis spectrophotometer. Transmission electron microscopic (TEM) images were acquired with a JEOL JEM-3010 high-resolution transmission electromicroscope using an accelerating voltage of 200 kV. TEM images were obtained at different parts of the grid and with different magnifications. X-ray diffraction (XRD) experiment was performed with a Shimadzu XD-3A X-ray diffractometer (Japan) using Cu-Ka radiation (k = 0.15418 nm). The scan rate was $4°\cdot min^{-1}$. Scanning electron microscopic (SEM) measurements were carried out on a scanning electron microscope (JEOL JSM-6700 F) at 20 kV. Samples were placed in aluminum stubs and were then coated with a gold layer by sputtering in order to enhance their conductivity.

2.3. Electrode preparation

A 1.0 wt.% CHIT solution was prepared by dissolving 1.0 g of CHIT into a 0.05 M acetic acid (HAc) and diluted with ultrapure water to form 1.0 wt.% solution, then was filtered using a 0.45 μm syringe filter unit. Prior to use, a glass carbon disk electrode (GCE, 3 mm in diameter, Model CHI104, CH Instruments, Austin, TX) was polished on a polishing cloth with alumina of successively smaller particles (0.3 μm and 0.05 μm diameter, respectively). Then the electrode was cleaned by ultrasonication in ethanol and ultrapure water, respectively. Typically, 2.0 mg TiC NPs was dispersed in 1.0 mL of CHIT solution (1.0 wt.%) with the help of ultrasonic agitation. Then, 2 mg of Mb was added into the above solution. The mixture was hand-mixed completely and was allowed to be left for overnight at 4 °C in a refrigerator. The H_2O_2 biosensor was constructed by coating a drop of 10 μL the resulting solution onto the modified electrode. The biosensor was stored at 4 °C in a refrigerator when not in use. A 0.1 M pH 7.0 sodium phosphate buffered (PB) solution was used in all electrochemical studies unless otherwise stated. Electrolyte solutions were purged with highly purified nitrogen for at least 20 min prior to experiments. A nitrogen atmosphere was then kept over solutions in the cell.

Electrochemical impedance spectra (EIS) were performed in 5.0 mM $K_3Fe(CN)_6$ + 5.0 mM $K_4Fe(CN)_6$ solution containing 0.2 M KCl. The impedance measurements were recorded at a bias potential of +205 mV (*vs.* SCE) within the frequency range of 10 mHz–10 kHz.

3. Results and discussion

3.1. Characterization of TiC NPs, Mb-TiC NPs-CHIT composite matrix and electrodes

Fig. 1A shows the XRD data of the TiC NPs. Analysis of the diffraction patterns reveal the presence of a number of diffraction features from TiC, corresponding to the (111), (200), and (220) crystal planes [32,34]. No diffraction features indicative of other forms of impurity phase were observed for TiC NPs. The shape of the diffraction peaks suggests that the sample could be well crystallized with small particle sizes. According to the Debye–Scherrer equation [42], the average crystallite size of the TiC NPs was calculated to be ca. 40 nm. Fig. 1B, C and D presents the SEM, TEM and particle distribution images of nanosized TiC. A histogram was obtained using the Nano Measurer 1.2 program to measure the diameter of each particle. It can be seen from the images that, sphere shape TiC NPs has uniform distribution with the size distribution ranging from 14 to 57 nm. The mean size and the standard deviation of the TiC NPs were 30.2 nm and 9.7 nm, respectively. The mean size is consisting with the result from XRD analysis.

To qualitatively investigate the biological activity of Mb before and after immobilization on TiC NPs-CHIT composite film, the changes of the Soret band were observed by monitoring the absorption band in the prosthetic heme–group region of the composite film [43,44]. As for Mb, the main characteristic peak located at about 400 nm is just the characteristic absorption of the porphyrin–Soret band. Curves in Fig. 2A showed the UV–vis spectra of Mb and Mb-TiC NPs-CHIT, respectively. As can be seen, the position and shape of adsorption bands (406 nm) for Mb in TiC NPs-CHIT composites (Fig. 2A, curve b) are almost the same as those for free Mb (406 nm), suggesting that Mb entrapped in the composite films has similar structures to the native state of Mb in PB solution. Moreover, a close inspection of the spectrum of free Mb and the Mb-TiC NPs-CHIT at about 503 nm [45], also supporting the conclusion that the Mb immobilized on TiC NPs-CHIT film indeed maintain its native structure.

It is well known that the amide I (1700 ~ 1600 cm^{-1}) and amide II (1620 ~ 1500 cm^{-1}) of heme-proteins can provide detailed information on the secondary structure of the polypeptide chain, so the Mb-TiC NPs/CHIT film is also studied by FTIR. As shown in Fig. 2B, the amide I and amide II bands of native Mb are located at 1654 and 1543 cm^{-1} in the FTIR spectrum (curve c), and the FTIR spectrum of Mb-TiC NPs/CHIT film (curve d) has similar shapes to that of native Mb, with the amide I and amide II bands only shifted slightly to 1650 and 1542 cm^{-1}, respectively. The results indicate that the secondary structure of Mb is kept as the native state of Mb and thus TiC NPs/CHIT composite matrix might provide an excellent platform for the study of the direct electrochemistry of Mb.

EIS is an effective method of probing the features of surface-modified electrodes, which provide useful information on the impedance changes of the electrode surface during the fabrication process [46,47]. Nyquist plot commonly include a semicircle region lying on the axis followed by a straight line. The semicircular part at higher frequencies corresponds to the electron-transfer-limited process and its diameter is equal to the electron transfer resistance (R_{et}), which controls the electron transfer kinetics of the redox probe at the electrode interface. Meanwhile, the linear part at lower frequencies corresponds to the diffusion process. Such spectra can be used for extracting the electron transfer kinetics and diffusional characteristics. The respective semicircles diameters at the high frequencies corresponding to the charge transfer resistance at the electrode surface. Thus, the charge transfer resistance was used as a sensor signal.

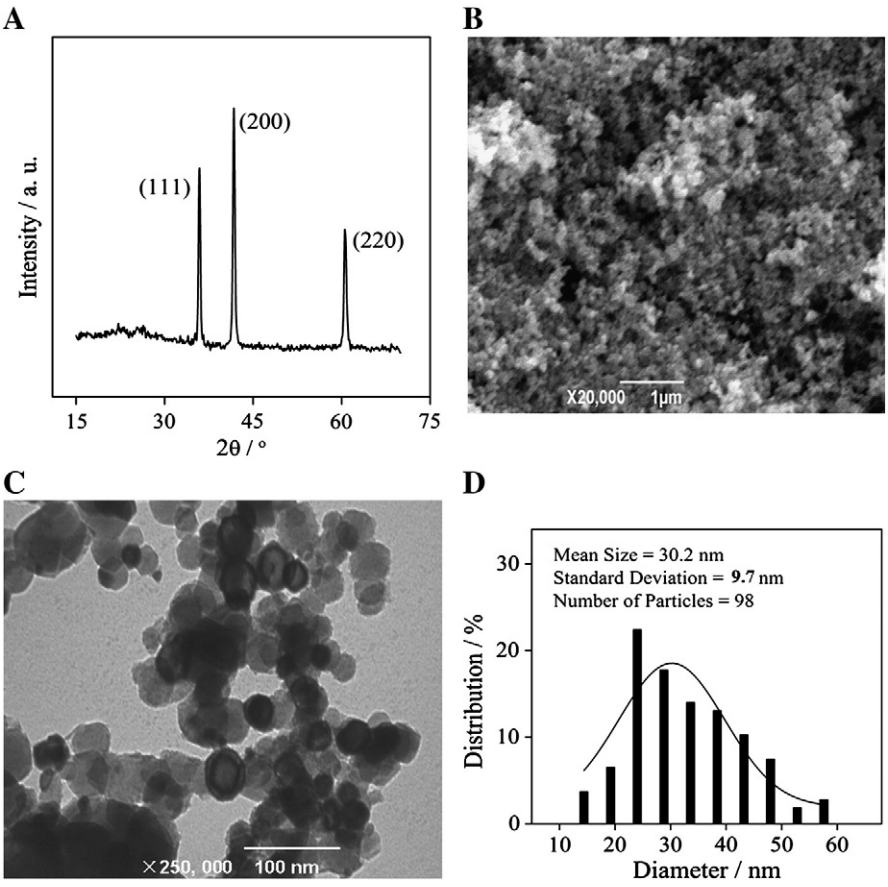

Fig. 1. (A) The X-ray diffraction spectrum of TiC NPs; (B) scanning electron microscopic, (C) transmission electron microscopic images TiC NPs and (D) particle size distribution histogram of TiC NPs.

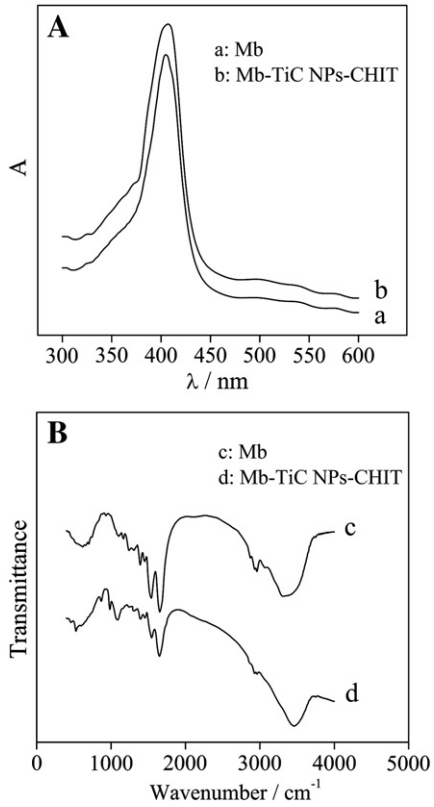

Fig. 2. (A) The UV–vis absorption spectra of Mb (curve a) and Mb-TiC NPs-CHIT (curve b); (B) Fourier-transform infrared spectra of Mb (curve c) and Mb-TiC NPs-CHI (curve d) composite film.

Fig. 3 displays the EIS of the GCE (a), CHIT/GCE (b), TiC NPs-CHIT/GCE (c) and Mb-TiC NPs-CHIT/GCE (d) in 5.0 mM 5.0 mM $K_3Fe(CN)_6$ + 5.0 mM $K_4Fe(CN)_6$ solution containing 0.2 M KCl. For bare GCE, a small semicircle of impedance plot is observed (curve a). After the GCE surface being modified by a CHIT layer, the EIS of the resulting electrode layer shows higher interfacial electron transfer resistance (curve b), indicating that the CHIT film obstruct the electron transfer of the redox probe. Decreased electron transfer resistance is observed when TiC NPs-CHIT is modified onto the GCE surface (curve c) compared with that of CHIT modified GCE, suggesting that the presence of TiC NPs enhances the conductivity of the modified film. When the Mb is immobilized on TiC NPs/CHIT/GCE (curves d), the semicircle of impedance plot is increased significantly, which further indicates that Mb is effectively immobilized in the composite film and further increase of the thickness of the composite film.

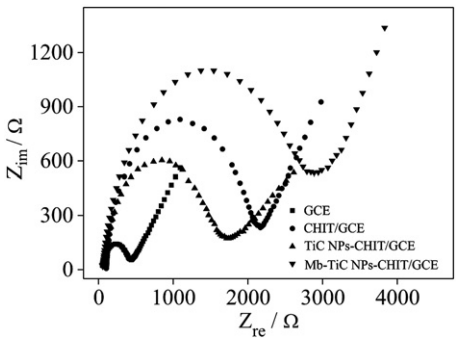

Fig. 3. Electrochemical impedance spectra of GCE (■), CHIT/GCE (●), TiC NPs-CHIT/GCE (▲) and Mb-TiC NPs-CHIT/GCE (▼) in 5.0 mM 5.0 mM $K_3Fe(CN)_6$ + 5.0 mM $K_4Fe(CN)_6$ solution containing 0.2 M KCl. Applied potential: +0.205 V (*vs.* SCE). Frequency range: 10 mHz–10 kHz.

3.2. Direct electrochemistry of Mb-TiC NPs-CHIT/GCE

The electrochemical behaviors of the Mb-TiC NPs-CHIT/GCE are examined by CV in 0.05 M pH 7.0 PB solution and the results are shown in Fig. 4. Bare GCE (curve a) does not show any peaks in the working potential range. As for the CHIT/GCE, also no peaks are observed (curve b). While at the Mb-CHIT/GCE, only very small redox peaks appeared in the voltammogram (curve c), this is possibly due to the unfavorable orientation of Mb molecules on the electrode surface. Only when TiC NPs was employed to immobilize Mb, there appeared a couple of quasi-reversible redox peaks of Mb corresponding to the active center of Mb Fe(III)/Fe(II) redox couple (curve d), suggesting that the presence of TiC NPs facilitate the electron transfer of Mb with the substrate electrode, and the direct electron transfer of Mb was achieved in the TiC NPs-CHIT composite film. The formal potential of Mb-TiC NPs-CHIT/GCE was −0.240 (±0.02) V (*vs.* SCE) and the peak to peak separation was 51 (±1) mV.

Fig. 5 is the CVs of the Mb-TiC NPs-CHIT/GCE obtained in 0.05 M PB solution (pH 7.0) solution at various scan rates. The values of ΔE_p are almost independent on the scan rates in the range of 100 to 1000 $mV \cdot s^{-1}$. Inset of Fig. 6A showed that the cathodic and anodic peaks current increases linearly with the increase of scan rates, suggesting the electrochemical reaction of the composite film modified electrode is a surface-controlled process. According to the equation $I_p = n^2F^2vA\Gamma/4RT$ [48], the surface coverage (Γ) of Mb on the electrode surface is estimated to be 5.86 (±0.32) × 10^{-10} $mol \cdot cm^{-2}$ from the slope of the I_p–v curve. This value is larger than or similar to previously reported values for Mb immobilized in other materials: collagen (1.1×10^{-10} $mol \cdot cm^{-2}$) [49], Fe_3O_4@Au composite (9.18×10^{-10} $mol \cdot cm^{-2}$) [50], TiO_2/MWCNT (8.35×10^{-11} $mol \cdot cm^{-2}$) [51] and $\{PEG/ZrO_2\}_6$ (2.5×10^{-10} $mol \cdot cm^{-2}$) [52] films, suggesting that the nanostructured TiC NPs provide a large surface area and a higher capability of composite TiC NPs-CHIT matrix for protein immobilization.

At higher scan rates, the plot of peak currents *vs.* scan rate deviated from linearity and the peak currents became proportional to the square root of the scan rates. On the other hand, the oxidation peak shifts to more positive potentials and the reduction peak shifts to more negative potentials (Fig. 5B). When $v \geq 2000$ $mV \cdot s^{-1}$, the values of cathodic and anodic peak potentials were proportional to the logarithm of the scan rate with slopes of $-2.3RT/\alpha nF$ and $2.3RT/(1-\alpha)nF$, respectively. The intrinsic mechanisms of electron transfer reactions, and the detailed role of the protein in aiding the electron transfer between redox centres, have become foci for extensive physical and biochemical investigations [53]. For example, the cell respiration involves the stepwise oxidation of organic substrates via a cascade of redox reactions. Thus measuring heterogeneous electron-transfer rates for Mb, it is possible to predict the magnitude of the

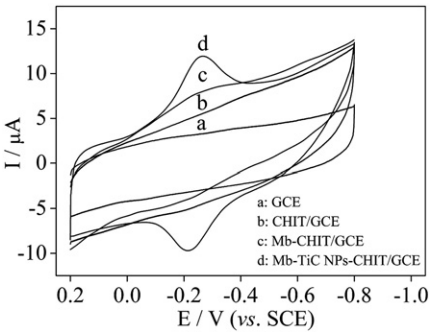

Fig. 4. Cyclic voltammograms of GCE (a), CHIT/GCE (b), Mb-CHIT/GCE (c), and Mb-TiC NPs-CHIT/GCE (d) in 0.05 M PB solution (pH 7.0) solution at a scan rate of 100 $mV \cdot s^{-1}$.

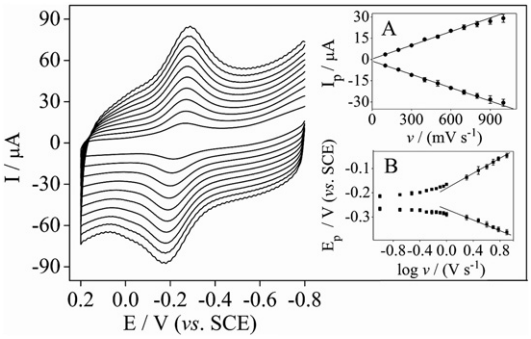

Fig. 5. Cyclic voltammograms of Mb-TiC NPs-CHIT/GCE in 0.05 M PB solution (pH 7.0) solution at various scan rates (from inner to outer curve): 100, 200, 300, 400, 500, 600, 700, 800, 900 and 1000 mV·s^{-1}. Insert graph: A) I_p/(μA) is presented as a function of ν/(mV·s^{-1}) ($\nu \leq 1000$ mV·s^{-1}); B) E_p/(V) is presented as a function of log ν/(V·s^{-1}) for the higher scan rates ($\nu > 1000$ mV·s^{-1}). Error bars represent the standard deviation for three independent measurements.

homogeneous electron-transfer rate from Mb to electrode surface. Based on the following Laviron equation, the electron transfer rate constant k_s as well as the transfer coefficient (α) was calculated.

$$\log k_s = \alpha\log(1-\alpha) + (1-\alpha)\log\alpha - \log(RT/nF\nu) - (1-\alpha)\alpha F\Delta E_p/(2.3RT) \quad (1)$$

Where α is electron transfer coefficient. n is the number of electron transfer. ΔE_p is the peak to peak potential separation. R, T and F symbols have their conventional meanings. The calculated value of k_s and α was about 3.8 ($\pm$0.2)·s^{-1} and 0.45, respectively. The value of k_s is much larger than the value obtained for Nafion/MWCNTs/CILE 0.332 s^{-1} [54], silk fibroin 1.34 s^{-1} [55], DNA/CILE 1.02 s^{-1} [56], and comparable for Fe_3O_4@Au 3.2 s^{-1} [50] and TiO_2/MWCNT 3.08 s^{-1} [51]. Therefore, TiC NPs can provide a good environment for Mb and facilitate the electron transfer of Mb, which may pave the way for elucidating the relationship between the heme-protein structures and biological functions.

3.3. Effect of pH values on the DET

The effect of pH values of the solution on the DET of the Mb-TiC NPs-CHIT/GCE was studied. Results show that an increase of pH value of the solution from pH 4.0 to 10.0 led to a negative shift of both reduction and oxidation peak potentials of the Mb-TiC NPs-CHIT/GCE. In general, all changes in the peak potentials and currents with the solution pH value were reversible in the pH value range from 4.0 to 10.0. That is, the same CVs could be obtained if the electrode was transferred from a solution with a different pH value to its original solution. The formal potential $E^{0'}$ has a linear relationship with pH values. The linear regression equation was obtained as $E^{0'}$/mV = 160.4 ($\pm$2.6)–57.2 ($\pm$1.2) pH (n = 7, r = 0.9982). The shift of $E^{0'}$ depending on pH value suggests that the redox reaction takes place accompanied by the transfer of proton. The slope (−57.2 ($\pm$1.2) mV·pH^{-1}) is close to that expected theoretically −59 mV·pH^{-1} for a one-electron one-proton reaction [57], indicating that a single proton transfer accompanied in the electrochemical process of Mb. The electrochemical reduction of Mb can be simply expressed as follows:

$$Mb[Fe^{III}] + e^- + H^+ \leftrightarrow Mb[H^+–Fe^{II}] \quad (1)$$

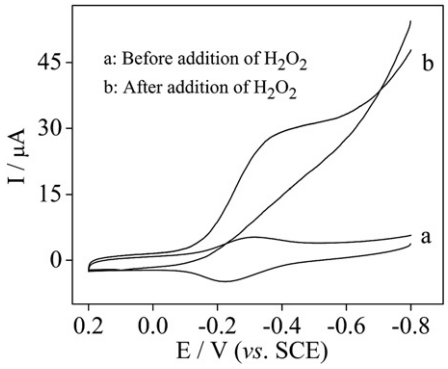

Fig. 6. Cyclic voltammograms of Mb-TiC NPs-CHIT/GCE before (curve a) and after (curve b) addition of 0.1 mL 0.1 M H_2O_2 to a 10.0 mL deoxygenated 0.05 M PB solution (pH 7.0).

3.4. Electrocatalytic ability of the Mb-TiC NPs-CHIT/GCE

It is well-known that proteins containing heme-groups, such as Hb, Mb, and HRP is able to reduce H_2O_2 electrocatalytically [15,49–52]. As shown in Fig. 6, when 0.1 mL 0.1 M H_2O_2 was added to a 10.0 mL deoxygenated pH 7.0 PB solution, the reduction peak of Mb-TiC NPs-CHIT/GCE increased dramatically at about −0.3 V. At the same time, the oxidation peak decreased (Fig. 6, curve b), demonstrating the typical electrocatalytic reduction process of H_2O_2. The catalytic procedures can be expressed as follows (compound I, denoted Mb[FeIVO•+]):

$$[Mb(Fe^{III})] + H_2O_2 \rightarrow \text{CompoundI} + H_2O \quad (2)$$

$$\text{CompoundI} + H_2O_2 \rightarrow [Mb(Fe^{III})] + H_2O + O_2 \quad (3)$$

$$[Mb(Fe^{III})] + H^+ + e^- \rightarrow [Mb(Fe^{II})]\text{atelectrode} \quad (4)$$

$$[Mb(Fe^{II})] + O_2 \rightarrow [Mb(Fe^{II})]–O_2\,\text{fast} \quad (5)$$

$$[Mb(Fe^{II})]–O_2 + H^+ + e^- \rightarrow [Mb(Fe^{III})] + H_2O_2\text{atelectrode} \quad (6)$$

The overall reaction of Eqs. (2)–(6) would be:

$$H_2O_2 + 2H^+ + 2e^- \rightarrow 2H_2O \quad (7)$$

The current–time amperometric curve is recorded under the conditions of continuous stirring of the solution and successive step changes of H_2O_2 concentration at −300 mV (*vs.* SCE) (as shown in Fig. 7A). When an aliquot of H_2O_2 is added into 0.05 M PB solution, the reductive current rises steeply to reach a stable value. The time to reach 90% of the maximum current is within 3 s, which indicates a fast response process. The H_2O_2 biosensor displays increasing amperometric responses to H_2O_2 with good linear range from 0.5 to 50.0 μM (Fig. 7B). The linear regression equation is I_{ss}/μA = 4.57 ($\pm$0.19) + 0.29 ($\pm$0.02)·$C(H_2O_2)$/μM with the correlation coefficient of 0.999. The linear response obtained with the biosensor covers the physiological concentration range of H_2O_2, such as in the plasma ranged from 13 to 57 μM [58] or the body fluid ranged from 25 to 60 μM [59], indicating that the biosensor can be possibly used in the analysis of human blood or body fluid samples. The detection limit was estimated at about 0.2 μM (S/N = 3). The linear range and detection limit obtained with the biosensor based on the Mb-TiC NPs-CHIT composite film are comparable with that of at Chit-MWNTs/Mb/AgNPs [60], Mb-MCFs [61], and {collagen/Mb}$_n$ [49] composite films. The sensitivity of Mb-TiC NPs-CHIT/GCE to H_2O_2 was found to be 4.08 ($\pm$0.03) μA·μM^{-1}·cm^{-2}. This value is higher than that of 0.59 μA·mM^{-1}·cm^{-2} at Chit-MWNTs/Mb/AgNPs/GCE (applied potential: −0.3 V (*vs.* Ag/AgCl)) [60], 0.43 μA·mM^{-1}·cm^{-2} at Mb-

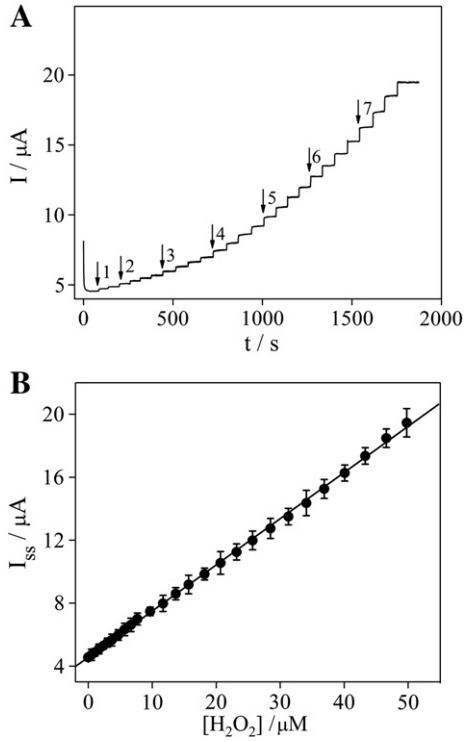

Fig. 7. (A) Amperometric responses of the Mb-TiC NPs-CHIT/GCE at −300 mV (*vs.* SCE) upon successive addition of H_2O_2 into a deoxygenated 0.05 M PB solution (pH 7.0); (B) I_{ss}/(μA) is presented as a function of $[H_2O_2]$/(μM). Error bars represent the standard deviation for three independent measurements.

MCFs/GCE (applied potential: −0.4 V (*vs.* Ag/AgCl)) [61], 0.25 $\mu A \cdot mM^{-1} \cdot cm^{-2}$ at Mb–TiO_2/MWCNTs/GCE (applied potential: −0.4 V (*vs.* SCE)) [51] and 1.62 $\mu A \cdot mM^{-1} \cdot cm^{-2}$ at Mb-HSG-SN-CNTs/GCE (applied potential: −0.45 V (*vs.* Ag/AgCl)) [62].

When the concentration of H_2O_2 was higher than 50.0 mM, the response curve tended to level off, demonstrating typical Michaelis–Menten kinetic characteristic of protein–based electrodes. The use of the Eadie–Hofstee form of the Michaelis–Menten equation is quite efficient in the kinetic analysis of the enzymatic reaction. For amperometric biosensors the reaction rates are substituted with steady-state current,

$$I_{ss} = I_{ss}^{max} - K_m^{app}(I_{ss}/C_{ss}) \quad (8)$$

Here I_{ss} is the steady-state current, C_{ss} the concentration of substrate, K_m^{app} is the apparent Michaelis–Menten constant, and I_{ss}^{max} is the intercept on the current axis [63]. The corresponding plot yielded an "apparent" K_m of 0.07 (±0.01) mM. The value is smaller or comparable than those reported for electrodes prepared by immobilizing Mb on Fe_3O_4@Au, 0.15 mM [50], TiO_2/MWCNTs, 0.08 mM [51], Fe_3O_4@Al_2O_3, 0.12 mM [64], DNA/CILE, 0.42 mM [56], and CILE, 0.14 mM [65], suggesting that Mb retained higher activity in the TiC NPs-CHIT film on the surface of GCE. The good microenvironment due to the synergistic effect of the hybrid composites might contribute to the improvement of the affinity and good performances of the biosensor.

3.5. Influences of pH and applied potential to the H_2O_2 determination

The pH influence on the electrocatalytic reduction of H_2O_2 at the Mb-TiC NPs-CHIT/GCE was investigated by measuring the current response of 5.0 μM H_2O_2 in the pH range from 4.0 to 10.0. Results showed that with solution pH increasing from 4.0 to 10.0, the current response of the Mb-TiC NPs-CHIT/GCE increased and reached a maximum value at pH 7.0. When the pH value is higher than 7.0, the slight decrease of amperometric response is observed, which may due to the denaturing of the immobilized Mb. Previous studies have demonstrated that the environmental electric field could lead to the changes of energy status of proteins and subsequently the forces, in particular the electrostatic interaction, to maintain the tertiary structure of proteins [66]. In pH 7.0 PBS solution, the Mb (pI = 7.2) slightly positively charged. Thus, even after considering the pI effect, the electrostatic interaction is expected to be weak and the electrostatic interaction while have little effect on the microenvironment around the heme site. So, pH 7.0 has been used throughout the experiments.

The effect of applied potential on the steady state current of the Mb-TiC NPs-CHIT/GCE showed that the electrocatalytic reduction of H_2O_2 could be observed at around −0.30 V. With applied potential decreasing from −0.1 V to −0.5 V, the steady state current increased due to the increased driving force for the fast reduction of H_2O_2 at the lower potentials and approached a maximum value at −0.3 V. Thus, −0.3 V was selected as the working potential for amperometric H_2O_2 determination.

3.6. Stability and reproducibility of the composite film modified electrode

The stability of the Mb-TiC NPs-CHIT composite film modified electrode is first evaluated by examining the cyclic voltammetric peak currents of Mb after continuously scanning for 50 cycles. No decrease of the voltammetric response is observed, indicating that the Mb-TiC NPs-CHIT composite film modified electrode is stable in buffer solution. The stability of the composite film modified electrode is also checked by measuring the current response of the Mb-TiC NPs-CHIT composite film modified electrode daily over a period of 30 days. When not in use, the electrode is stored dry at 4 °C in a refrigerator. It is found that the composite film modified electrode maintain its 92% initial activity after 30 days. Conversely, without the presence of TiC NPs, the current response of the Mb-CHIT modified electrode decreased dramatically and maintains its 65% initial activity after 7 days, after which, the composite film was easily collapsed and falls off from electrode surface. The above results indicated that the TiC NPs could greatly improve the composite film stably attached on the GCE surface. The repeatability and reproducibility of the biosensor were determined. The repeatability of one electrode was conducted by adding 10 μL of 1.0 mM H_2O_2 into a 20 mL 0.05 M PB solution. The relative standard deviation was 3.6% for 8 successive assays. Five Mb-TiC NPs-CHIT/GCEs prepared by following identical steps was used to estimate the reproducibility of the biosensor by measuring the current responses of the Mb-TiC NPs-CHIT/GCEs to 5.0 μM H_2O_2. The relative standard deviation was 5.7%.

4. Conclusions

In the present work, the direct electrochemistry of Mb fabricated by using a composite matrix based on CHIT and TiC NPs was achieved. Compared with the absence of TiC NPs used for fabricate the biosensor, the presence of TiC NPs accelerated the DET rate between Mb and the substrate electrode significantly. The resulting biosensor showed excellent electrocatalytic activity towards the reduction of H_2O_2 with a wider linearity range and a lower detection limits. The excellent performances of the resulting biosensor maybe that the combining of CHIT and TiC NPs substantially improve the protein stability. The promising feature of the biocompatible hybrid materials could serve as a versatile platform for the fabrication of electrochemical biosensors.

Acknowledgements

The authors gratefully acknowledge the financial support of this project by the National Science Foundation of China (No. 20875076

and 21105080) and the Education Department of Shaanxi Province, China (No. 2010JK877).

References

[1] A. Brajter-Toth, J.Q. Chambers, Electroanalytical Methods for Biological Materials, Marcel Dekker, New York, 2002.
[2] J.J. Gooding, R. Wibowo, J. Liu, W. Yang, D. Losic, S. Orbons, F.J. Mearns, J.G. Shapter, D.B. Hibbert, Protein electrochemistry using aligned carbon nanotube arrays, J. Am. Chem. Soc. 125 (2003) 9006–9007.
[3] P.V. Bernhardt, G. Schenk, G.J. Wilson, Direct electrochemistry of porcine purple acid phosphatase (Uteroferrin), Biochemistry 43 (2004) 10387–10392.
[4] G.S. Pulcu, B.L. Elmore, D.M. Arciero, A.B. Hooper, S.J. Elliott, Direct electrochemistry of tetraheme cytochrome c554 from *Nitrosomonas europaea*: redox cooperativity and gating, J. Am. Chem. Soc. 129 (2007) 1838–1839.
[5] S.J. Sadeghi, R. Meirinhos, G. Catucci, V.R. Dodhia, G. Di Nardo, G. Gilardi, Direct electrochemistry of drug metabolizing human flavin-containing monooxygenase: electrochemical turnover of Benzydamine and Tamoxifen, J. Am. Chem. Soc. 132 (2010) 458–459.
[6] A.P. Periasamy, Y.J. Chang, S.M. Chen, Amperometric glucose sensor based on glucose oxidase immobilized on gelatin-multiwalled carbon nanotube modified glassy carbon electrode, Bioelectrochemistry 80 (2011) 114–120.
[7] F. Scheller, F. Schubert, Biosensors, Elsevier, Amsterdam, 1992.
[8] A.J. Cunningham, Introduction to Bioanalytical Sensors, John Wiley & Sons Inc., New York, 1998.
[9] G.C. Zhao, L. Zhang, X.W. Wei, An unmediated H_2O_2 biosensor based on the enzyme-like activity of myoglobin on multi-walled carbon nanotubes, Anal. Biochem. 329 (2004) 160–161.
[10] Z.J. Wang, M.Y. Li, P.P. Su, Y.J. Zhang, Y.F. Shen, D.X. Han, A. Ivaska, L. Niu, Direct electron transfer of horseradish peroxidase and its electrocatalysis based on carbon nanotube/thionine/gold composites, Electrochem. Commun. 10 (2008) 306–310.
[11] G.S. Lai, H.L. Zhang, D.Y. Han, Amperometric hydrogen peroxide biosensor based on the immobilization of horseradish peroxidase by carbon-coated iron nanoparticles in combination with chitosan and cross-linking of glutaraldehyde, Microchim. Acta 165 (2009) 159–165.
[12] S.X. Xu, X.F. Zhang, T. Wan, C.X. Zhang, A third-generation hydrogen peroxide biosensor based on horseradish peroxidase cross-linked to multi-wall carbon nanotubes, Microchim. Acta 172 (2011) 199–205.
[13] W.M. Li, Z. Shi, N. Li, Z. Gu, Direct electrochemistry of cytochrome c at a glassy carbon electrode modified with single-wall carbon nanotubes, Anal. Chem. 74 (2002) 1993–1997.
[14] W. Sun, X.Q. Li, Y. Wang, R.J. Zhao, K. Jiao, Electrochemistry and electrocatalysis of hemoglobin on multi-walled carbon nano-tubes modified carbon ionic liquid electrode with hydrophilic $EMIMBF_4$ as modifier, Electrochim. Acta 54 (2009) 4141–4148.
[15] J.J. Feng, J.J. Xu, H.Y. Chen, Synergistic effect of zirconium phosphate and Au nanoparticles on direct electron transfer of hemoglobin on glassy carbon electrode, J. Electroanal. Chem. 585 (2005) 44–50.
[16] G.C. Zhao, Z.Z. Yin, L. Zhang, X.W. Wei, Direct electrochemistry of cytochrome c on a multi-walled carbon nanotubes modified electrode and its electrocatalytic activity for the reduction of H_2O_2, Electrochem. Commun. 7 (2005) 256–260.
[17] L. Qian, X. Yang, Composite film of carbon nanotubes and chitosan for preparation of amperometric hydrogen peroxide biosensor, Talanta 68 (2006) 721–727.
[18] Y.L. Zhou, Z. Li, N.F. Hu, Y.H. Zeng, J.F. Rusling, Layer-by-layer assembly of ultrathin films of hemoglobin and clay nanoparticles with electrochemical and catalytic activity, Langmuir 18 (2002) 8573–8579.
[19] M.H. Yang, Y.H. Yang, B. Liu, G.L. Shen, R.Q. Yu, Amperometric glucose biosensor based on chitosan with improved selectivity and stability, Sens. Actuators B 101 (2004) 269–276.
[20] H. Huang, N.F. Hu, Y.H. Zeng, G. Zhou, Electrochemistry and electrocatalysis with heme proteins in chitosan biopolymer films, Anal. Biochem. 308 (2002) 141–151.
[21] D. Shan, S.X. Wang, H.G. Xue, S. Cosnier, Direct electrochemistry and electrocatalysis of hemoglobin entrapped in composite matrix based on chitosan and $CaCO_3$ nanoparticles, Electrochem. Commun. 9 (2007) 529–534.
[22] Q. Xu, C. Mao, N.N. Liu, J.J. Zhu, J. Sheng, Direct electrochemistry of horseradish peroxidase based on biocompatible carboxymethyl chitosan-gold nanoparticle nanocomposite, Biosens. Bioelectron. 22 (2006) 768–773.
[23] C.S. Shan, H.F. Yang, J.F. Song, D.X. Han, A. Ivaska, L. Niu, Direct electrochemistry of glucose oxidase and biosensing for glucose based on graphene, Anal. Chem. 81 (2009) 2378–2382.
[24] Z.F. Deng, Q. Rui, X. Yin, H.Q. Liu, Y. Tian, In vivo detection of superoxide anion in bean sprout based on ZnO nanodisks with facilitated activity for direct electron transfer of superoxide dismutase, Anal. Chem. 80 (2008) 5839–5846.
[25] X.L. Xiao, Q.F. Luan, X. Yao, K.B. Zhou, Single-crystal CeO_2 nanocubes used for the direct electron transfer and electrocatalysis of horseradish peroxidase, Biosens. Bioelectron. 24 (2009) 2447–2451.
[26] X. Xu, B.Z. Tian, S. Zhang, J.L. Kong, D.Y. Zhao, B.H. Liu, Electrochemistry and biosensing reactivity of heme proteins adsorbed on the structure-tailored mesoporous Nb_2O_5 matrix, Anal. Chim. Acta 519 (2004) 31–38.
[27] Z.F. Deng, Y.C. Gong, Y.P. Luo, Y. Tian, WO_3 Nanostructures facilitate electron transfer of enzyme: application to detection of H_2O_2 with high selectivity, Biosens. Bioelectron. 24 (2009) 2465–2469.
[28] C.P. You, X.W. Yan, J.L. Kong, D.Y. Zhao, B.H. Liu, Direct electrochemistry of myoglobin based on bicontinuous gyroidal mesoporous carbon matrix, Electrochem. Commun. 10 (2008) 1864–1867.
[29] Q.L. Sheng, K. Luo, L. Li, J.B. Zheng, Direct electrochemistry of glucose oxidase immobilized on $NdPO_4$ nanoparticles/chitosan composite film on glassy carbon electrodes and its biosensing application, Bioelectrochemistry 74 (2009) 246–253.
[30] H.H. Hwu, J.G. Chen, Surface chemistry of transition metal carbides, Chem. Rev. 105 (2005) 185–212.
[31] T. Yu, Y.H. Deng, L. Wang, R.L. Liu, L.J. Zhang, B. Tu, D.Y. Zhao, Ordered mesoporous nanocrystalline titanium-carbide/carbon composites from in situ carbothermal reduction, Adv. Mater. 19 (2007) 2301–2306.
[32] D.W. Flaherty, R.A. May, S.P. Berglund, K.J. Stevenson, C.B. Mullins, Low temperature synthesis and characterization of nanocrystalline titanium carbide with tunable porous architectures, Chem. Mater. 22 (2010) 319–329.
[33] J.A. Rodríguez, L. Feria, T. Jirsak, Y. Takahashi, K. Nakamura, F. Illas, Role of Au-C interactions on the catalytic activity of Au nanoparticles supported on TiC(001) toward molecular oxygen dissociation, J. Am. Chem. Soc. 132 (2010) 3177–3186.
[34] S.V. Didziulis, H.I. Kim, Chemistry of methyl formate with TiC(100): comparison of experiment with density functional calculations, J. Phys. Chem. C 111 (2007) 11275–11284.
[35] B. Bas, R. Piech, E. Niewiara, M. Ziemnicka, L. Stobierski, W.W. Kubia, TiC working electrode: voltammetric characteristics and application for determination of lead traces by stripping voltammetry, Electroanalysis 20 (2008) 1655–1664.
[36] V. Kiran, S.B. Kalidindi, B.R. Jagirdar, S. Sampath, Electrochemical oxidation of boron containing compounds on titanium carbide and its implications to direct fuel cells, Electrochim. Acta 56 (2011) 10493–10499.
[37] H.J. Liu, J. Wang, C.X. Wang, Y.Y. Xia, Ordered hierarchical mesoporous/microporous carbon derived from mesoporous titanium-carbide/carbon composites and its electrochemical performance in supercapacitor, Adv. Energy Mater. 1 (2011) 1101–1108.
[38] M. Brama, N. Rhodes, J. Hunt, A. Ricci, R. Teghil, S. Migliaccio, C.D. Rocca, S. Leccisotti, A. Lioi, M. Scandurra, G.D. Maria, D. Ferro, F. Pu, G. Panzini, L. Politi, R. Scandurra, Effect of titanium carbide coating on the osseointegration response in vitro and in vivo, Biomaterials 28 (2007) 595–608.
[39] M. Rosenbaum, F. Zhao, U. Schröder, F. Scholz, Interfacing electrocatalysis and biocatalysis with tungsten carbide: a high-performance, noble-metal-free microbial fuel cell, Angew. Chem. Int. Ed. 45 (2006) 6658–6661.
[40] K. Fujita, N. Nakamura, H. Ohno, B.S. Leigh, K. Niki, H.B. Gray, J.H. Richards, J. Am. Chem. Soc. 126 (2004) 13954–13961.
[41] C. Léger, P. Bertrand, Direct electrochemistry of redox enzymes as a tool for mechanistic studies, Chem. Rev. 108 (2008) 2379–2438.
[42] H. Klug, L. Alexander, X-ray Diffraction Procedures, Wiley, New York, 1962, p. 125.
[43] X.B. Lu, J.Q. Hu, X. Yao, Z.P. Wang, J.H. Li, Composite system based on chitosan and room-temperature ionic liquid: direct electrochemistry and electrochemistry and electrocatalysis of hemoglobin, Biomacromolecules 7 (2006) 975–980.
[44] P. George, G.A. Hanania, Spectrophotometric study of ionizations in methemoglobin, J. Biochem. 55 (1953) 236–243.
[45] R. Quinn, J.M. Smith, J.N. Burstyn, Influence of hydrogen bonding on the properties of iron porphyrin imidazole complexes. An internally hydrogen bonded imidazole ligand, J. Am. Chem. Soc. 106 (1984) 4136–4144.
[46] R. Ehret, W. Baumann, M. Brischwein, A. Schwinde, K. Stegbauer, B. Wolf, Monitoring of cellular behaviour by impedance measurements on interdigitated electrode structures, Biosens. Bioelectron. 12 (1997) 29–41.
[47] X.J. Liu, Y.X. Huang, W.J. Zhang, G.F. Fan, C.H. Fan, G.X. Li, Electrochemical investigation of redox thermodynamics of immobilized myoglobin: ionic and ligation effects, Langmuir 21 (2005) 375–378.
[48] E. Laviron, The use of linear potential sweep voltammetry and of AC voltammetry for the study of the surface electrochemical reaction of strongly adsorbed systems and of redox modified electrodes, J. Electroanal. Chem. 100 (1979) 263–270.
[49] X. Miao, Y. Liu, W.C. Gao, N.F. Hu, Layer-by-layer assembly of collagen and electroactive myoglobin, Bioelectrochemistry 79 (2010) 187–192.
[50] J.D. Qiu, H.P. Peng, R.P. Liang, X.H. Xia, Facile preparation of magnetic core–shell Fe_3O_4@Au nanoparticle/myoglobin biofilm for direct electrochemistry, Biosens. Bioelectron. 25 (2010) 1447–1453.
[51] L. Zhang, D.B. Tian, J.J. Zhu, Direct electrochemistry and electrochemical catalysis of myoglobin–TiO_2 coated multiwalled carbon nanotubes modified electrode, Bioelectrochemistry 74 (2008) 157–163.
[52] K. Qiao, N.F. Hu, Direct electron transfer and electrocatalysis of myoglobin loaded in layer-by-layer films assembled with nonionic poly(ethylene glycol) and ZrO_2 nanoparticles, Bioelectrochemistry 75 (2009) 71–76.
[53] J.I. Blankman, N. Shahzad, C.J. Miller, R.D. Guiles, Direct voltammetric investigation of the electrochemical properties of human hemoglobin: relevance to physiological redox chemistry, Biochemistry 39 (2000) 14806–14812.
[54] W. Sun, X.Q. Li, Y. Wang, X. Li, C.Z. Zhao, K. Jiao, Electrochemistry of myoglobin in Nafion and multi-walled carbon nanotubes modified carbon ionic liquid electrode, Bioelectrochemistry 75 (2009) 170–175.
[55] Y.H. Wu, Q.C. Shen, S.S. Hu, Direct electrochemistry and electrocatalysis of hemeproteins in regenerated silk fibroin film, Anal. Chim. Acta 558 (2006) 179–186.
[56] R.F. Gao, J.B. Zheng, Direct electrochemistry of myoglobin based on DNA accumulation on carbon ionic liquid electrode, Electrochem. Commun. 11 (2009) 1527–1529.
[57] H. Jun, G. Hedayatollah, A.A. Moosavi-Movahedi, Direct electron transfer of redox proteins on a Nafion-cysteine modified gold electrode, Electrochem. Commun. 8 (2006) 1572–1576.

[58] G. Bleau, C. Giasson, I. Brunette, Measurement of hydrogen peroxide in biological samples containing high levels of ascorbic acid, Anal. Biochem. 263 (1998) 13–17.
[59] S.D. Varma, P.S. Devamanoharn, Hydrogen peroxide in human blood, Free Radic. Res. Commun. 14 (1991) 125–131.
[60] Y.C. Li, Y.J. Li, Y.Y. Yang, Direct electrochemistry and electrocatalysis of myoglobin-based nanocomposite membrane electrode, Bioelectrochemistry 82 (2011) 112–116.
[61] L. Zhang, Q. Zhang, J.H. Li, Direct electrochemistry and electrocatalysis of myoglobin covalently immobilized in mesopores cellular foams, Biosens. Bioelectron. 26 (2010) 846–849.
[62] C.Y. Liu, J.M. Hu, Hydrogen peroxide biosensor based on the direct electrochemistry of myoglobin immobilized on silver nanoparticles doped carbon nanotubes film, Biosens. Bioelectron. 24 (2009) 2149–2154.
[63] R.A. Kamin, G.S. Wilson, Rotating ring-disk enzyme electrode for biocatalysis kinetic studies and characterization of the immobilized enzyme layer, Anal. Chem. 52 (1980) 1198–1205.
[64] H.P. Peng, R.P. Liang, J.D. Qiu, Facile synthesis of Fe_3O_4@Al_2O_3 core–shell nanoparticles and their application to the highly specific capture of heme proteins for direct electrochemistry, Biosens. Bioelectron. 26 (2011) 3005–3011.
[65] X.D. Shangguan, J.B. Zheng, Direct electron transfer and electrocatalysis of myoglobin based on its direct immobilization on carbon ionic liquid electrode, Electroanalysis 21 (2009) 881–886.
[66] J.M. Vanderkooi, The protein state of matter, Biochim. Biophys. Acta 1386 (1998) 241–253.

Minzhi Wang is a graduate student of Institute of Analytical Science, Northwest University, China. The current research interest is enzyme-based biosensor.

Qinglin Sheng is a Lecturer of Institute of Analytical Science, Northwest University, China. He received his Doctor Degree from Northwest University, China, in 2009. The current research interests are electroanalysis and electrochemical biosensor.

Dawei Zhang is a graduate student of Institute of Analytical Science, Northwest University, China. The current research interest is enzyme-based biosensor.

Yaping He is a Doctoral student of Institute of Analytical Science, Northwest University, China. The current research interest is synthesis of nanomaterials and its application in biosensors.

Jianbin Zheng is a professor of Institute of Analytical Science, Northwest University, China. He obtained his Ph. D. in 1997 at the Department of Chemistry of Northwest University, China. He finished his Postdoctoral work in 2000 in Xi'an Institute of Optics and Precision Mechanics, Chinese Academy of Sciences, China. His research interests include electroanalytical chemistry, electrochemical biosensor, ionic liquid electrochemistry, HPLC electrochemistry and chemometrics.